symmetry

MDPI

Article

Synthesis, X-ray Diffraction and Computational Druglikeness Evaluation of New Pyrrolo[1,2-a][1,10]Phenanthrolines Bearing a 9-Cyano Group

Mihaela Cristea [1], Marcel Mirel Popa [1,*], Sergiu Shova [2], Maria Gdaniec [3], Amalia Stefaniu [4], Constantin Draghici [1], Mihai Raduca [1,5], Nicoleta Doriana Banu [1] and Florea Dumitrascu [1,*]

1 "C. D. Nenițescu" Institute of Organic and Supramolecular Chemistry, Romanian Academy, 202 B Splaiul Independenței, 060023 Bucharest, Romania; mihcris2012@yahoo.ro (M.C.); cst_drag@yahoo.com (C.D.); fiidemn@gmail.com (M.R.); doriana.banu@yahoo.com (N.D.B.)
2 Department of Inorganic Polymers, Petru Poni Institute of Macromolecular Chemistry, Aleea Grigore Ghica Vodă nr. 41A, 700487 Iaşi, Romania; shova@icmpp.ro
3 Faculty of Chemistry, Adam Mickiewicz University, 61-614 Poznań, Poland; magdan@amu.edu.pl
4 National Institute of Chemical Pharmaceutical Research and Development—ICCF, 112 Vitan Av., 031299 Bucharest, Romania; astefaniu@gmail.com
5 Inorganic Chemistry Department, Faculty of Chemistry, University of Bucharest, Regina Elisabeta Blvd., 4-12, 030018 Bucharest, Romania
* Correspondence: mirelupb@gmail.com (M.M.P.); fdumitra@yahoo.com (F.D.)

Abstract: New 9-cyano-pyrrolo[1,2-a][1,10]phenanthrolines **5a–d**, obtained by a 1,3-dipolar cycloaddition reaction between the corresponding N-ylides of 1,10-phenanthrolinium bromides **2a–d**, generated in situ and acrylonitrile as a dipolarophile, were investigated by single-crystal X-ray diffraction and computational studies to assess their druglikeness and evaluate their structure-activity properties. The non-covalent interactions present within the supramolecular landscape of the new 9-cyano-pyrrolo[1,2-a][1,10]phenanthrolines were correlated with the SAR investigations with the aim of estimating the propensity for bioactivity in these compounds.

Keywords: pyrrolo[1,2-a][1,10]phenanthroline; 1,3-dipolar cycloaddition; crystal structure; helical chirality; DFT; druglikeness; solvate

Citation: Cristea, M.; Popa, M.M.; Shova, S.; Gdaniec, M.; Stefaniu, A.; Draghici, C.; Raduca, M.; Banu, N.D.; Dumitrascu, F. Synthesis, X-ray Diffraction and Computational Druglikeness Evaluation of New Pyrrolo[1,2-a][1,10]Phenanthrolines Bearing a 9-Cyano Group. *Symmetry* **2024**, *16*, 911. https://doi.org/10.3390/sym16070911

Academic Editor: Takashi Mino

Received: 28 June 2024
Revised: 12 July 2024
Accepted: 15 July 2024
Published: 17 July 2024

1. Introduction

The derivatives of fused polyazaheterocycles, known for their wide range of biological activities, are of considerable interest due to their extensive applications in medicinal chemistry [1]. In order to increase the structural diversity of biologically active compounds, through structural combination strategies that aim to assemble different pharmacophores in the same molecular framework, several series of fused pyrrolophenanthrolines have been reported so far in the literature as possessing both biological impact and other interesting properties [2].

Fused pyrrolo[1,10]phenanthroline derivatives have attracted the attention of researchers, with the chemistry, synthesis methods and properties of these N-heterocycles being studied by several research groups [3–7]. These polycyclic compounds are very interesting molecules, with biological [8–14], electrical [15–17] or optical [18,19] properties.

The great potential of functionalization of phenanthroline or chemical transformation to more complex polycyclic compounds is also known, one example being their utilization in the obtaining of helicenes, polycyclic compounds displaying helical chirality [20–29].

Our on-going objective was the application of 1,3-dipolar cycloaddition of cycloimmonium *N*-ylides to obtain pyrrolo-fused nitrogen heterocycles, and thus phenanthroline was a remarkable building block for constructing interesting new structures [10,20,24–27,30–37]. The synthesis of such structures is rather limited to a few strategies [2,21,26,34,38–44].

The literature data show few reports on the biological activity of pyrrolo[1,2-a][1,10] phenanthroline derivatives [37,45]. Moreover, the cyano group is among the interesting pharmacophores to be investigated [46–48].

In silico investigations on physicochemical properties and pharmacokinetics are widely employed in medicinal chemistry to assess the potential of a small molecule to become an active therapeutic agent against specific targets, depending on their interaction strengths and binding affinity. Density Functional Theory (DFT) methods are used to predict properties [49] and key molecular descriptors and parameters related to pharmacokinetics and bioavailability [50,51] to rationally design new molecules with enhanced potential and specificity against various diseases. In drug development, the pharmacokinetics properties, such as absorption, distribution, metabolism and excretion (ADME profile), of drug candidates can be predicted using computational tools for specific molecular parameters which must comply with pre-established rules [52,53].

Herein we present some structural aspects of nitrile functionalized pyrrolo[1,2-*a*][1,10] phenanthroline, which can indicate their potential for in-depth pharmaceutical screening based on the nitrile pharmacophore group, their binding properties and non-covalent interactions of such compounds extracted from their interesting crystallographic structures.

2. Materials and Methods

2.1. Chemicals and Instrumentations

Melting points were measured on a Boëtius hot plate apparatus and are uncorrected. The ^{1}H and ^{13}C-NMR spectra were recorded on a Varian Gemini 300 BBat 300 MHz for ^{1}H and 75 MHz for ^{13}C. Chemical shifts (δ) are given in parts per million (ppm); the homo- and heterocoupling patterns (J) are given in hertz (Hz). The chemical shifts were measured against the residual solvent peak as reference.

All starting materials or solvents are commercially available and were used without further purification.

2.2. Synthesis and Characterization of Compounds **5a–c**

Synthesis of 9-cyano-pyrrolo[1,2-a][1,10]phenanthrolines:

A mixture of 1,10-phenanthrolinium bromide **2a–c** (5 mmol), acrylonitrile (15 mmol), and Et_3N (6 mmol) and tetrakis-pyridino-cobalt (II) dichromate (TPCD, 5 mmol) in DMF (30 mL) was stirred at 80–90 ∘C for 6 h. After cooling the resulting mixture to room temperature, a 5% (*v*/*v*) aqueous HCl solution (100 mL) was added. Compounds **5a–c** were obtained as precipitates, filtered and subsequently purified by crystallization from nitromethane, resulting in the 9-cyano-pyrrolo[1,2-*a*][1,10]phenanthrolines **5a–c** in good yields.

*11-(4-Methylbenzoyl)pyrrolo[1,2-a][1,10]phenanthroline-9-carbonitrile (***5a***)*

Yellow platelet-shaped crystals obtained from acetonitrile, m.p. 259–261 °C; yield 57%. Elemental analysis: found for $C_{24}H_{15}N_3O$: C, 79.98; H, 4.51; N, 11.92. Calculated: C, 79.76; H, 4.18; N, 11.63. ^{1}H-NMR ($CDCl_3$; δ, ppm; J, Hz): 2.51 (s, 3H, Me); 7.34–7.41 (m, 4H, H-3, H-10, H-3′, H-5′); 7.74 (d, 1H, 9.1, H-7); 7.85 (d, 1H, 8.5, H-5); 7.90 (d, 1H, 8.5, H-6); 7.92 (d, 1H, 9.1, H-8); 8.10–8.24 (m, 4H, H-2, H-4, H-2′, H-6′). ^{13}C-NMR ($CDCl_3$; δ, ppm): 21.8 (Me); 84.9 (C-9); 116.0 (CN); 117.8 (C-8); 121.2 (C-10); 122.8 (C-3); 125.5, 127.8, 129.6, 133.5, 137.7, 140.6 (C-4a, C-6a, C-8a, C-11, C-12a, C-12b); 125.6 (C-5); 126.0 (C-6); 126.5 (C-7); 129.2 (C-3′, C-5′); 130.3 (C-2′, C-6′); 134.4 (C-1′); 143.6 (C-4′); 135.9 (C-4); 146.3 (C-2); 184.4 (CO).

*11-(Biphenylcarbonyl)pyrrolo[1,2-a][1,10]phenanthroline-9-carbonitrile (***5b***)*

Yellow platelet-shaped crystals obtained from acetonitrile, m.p. 231–233 °C; yield 50%. Elemental analysis: found for $C_{29}H_{17}N_3O$: C, 82.63; H, 4.39; N, 10.33. Calculated: C, 82.25; H, 4.05; N, 9.92. ^{1}H-NMR ($CDCl_3$; δ, ppm; J, Hz): 7.39–7.54 (m, 5H, H-3, H-10, H-3″, H-4″, H-5″); 7.71–7.96 (m, 8H, H-5, H-6, H-7, H-8, H-3′, H-5′, H-2″, H-6″); 8.21–8.31 (m, 4H, H-2, H-4, H-2′, H-6′).^{13}C-NMR ($CDCl_3$; δ, ppm): 85.2 (C-9); 116.0 (CN); 118.0 (C-8); 121.5 (C-10); 122.9 (C-3); 125.7, 128.0, 129.5, 133.5, 137.8, 140.7 (C-4a, C-6a, C-8a, C-11, C-12a, C-12b); 125.7 (C-5); 126.1 (C-6); 126.7 (C-7); 127.2 (C-3″, C-5″); 127.5 (C-2″, C-6″); 128.4 (C-4″); 129.2 (C-3′, C-5′); 130.9 (C-2′, C-6′); 135.9 (C-1′); 136.1 (C-4); 140.2 (C-1″); 145.6 (C-4′); 146.5 (C-2); 184.2 (CO).

*11-(4-Nitrobenzoyl)pyrrolo[1,2-a][1,10]phenanthroline-9-carbonitrile (***5c***)*

Yellow platelet-shaped crystals obtained from acetonitrile, m.p. 315–317 °C; yield 55%. Elemental analysis: found for $C_{23}H_{12}N_4O_3$: C 70.70; H 3.39; N 14.55. Calculated: C, 70.41; H, 3.08; N, 14.28. ^{1}H-NMR ($CDCl_3$; δ, ppm; J, Hz): 7.36 (s, 1H, H-10); 7.45 (dd, 1H, 8.2, 4.4., H-3); 7.82 (d, 1H, 9.1, H-7); 7.91 (d, 1H, 8.8, H-5); 7.97 (d, 1H, 9.4, H-6); 8.00 (d, 1H, 9.4, H-8); 8.20 (dd, 1H, 4.4, 1.5, H-2); 8.27 (dd, 1H, 8.2, 1.5, H-4); 8.34 (d, 2H, 8.8, H-2′, H-6′); 8.40 (d, 2H, 8.8, H-3′, H-5′). ^{13}C-NMR ($CDCl_3$; δ, ppm): 85.8 (C-9); 115.6 (CN); 118.1 (C-8); 121.5 (C-10); 123.2 (C-3); 123.9 (C-3′, C-5′); 125.8; 128.2; 129.5; 132.3; 137.4; 140.9 (C-4a; C-6a; C-8a; C-11; C-12a; C-12b); 125.8 (C-5); 126.6 (C-6); 126.9 (C-7); 131.0 (C-2′, C-6′); 136.5 (C-4); 142.4 (C-1′); 146.3 (C-2); 150.4 (C-4′); 183.8 (CO).

2.3. X-ray Structural Analysis

Single-crystal X-ray diffraction data were collected by a XtaLAB Synergy, Dualflex, and HyPix diffractometer using Cu Kα radiation. The unit cell determination and data integration were carried out using the CrysAlisPro package from Oxford Diffraction [54]. The multi-scan correction for absorption was applied. The structures were solved with the SHELXT program using the intrinsic phasing method and refined by the full-matrix least-squares method on F^2 with SHELXL [55,56]. Olex2 was used as an interface to the SHELX programs [57]. An anisotropic model was used for the refinement of non-hydrogen atoms. Hydrogen atoms were added in idealized positions and refined using a riding model. Compound **5b** was crystallized as a chloroform semisolvate which was encountered before for similar structures [21]. The crystal structures are reported for two triclinic solid-state phases of this compound, the room temperature phase **5bHT** and low temperature phase **5bLT** at 160 K. Upon cooling, the disordered solvent molecule became ordered and the unit cell volume doubled. Selected crystallographic data and structure refinement details are provided in Table 1 and the corresponding CIF files. The supplementary crystallographic data can be obtained free of charge via www.ccdc.cam.ac.uk/conts/retrieving.html (or from the Cambridge Crystallographic Data Centre, 12 Union Road, Cambridge CB2 1EZ, UK; fax: (+44) 1223-336-033; or deposit@ccdc.ca.ac.uk).

Table 1. Crystal data and details of structure refinement for **5a**, **5bHT**, **5bLT** and **5c**.

Compound	**5a**	**5bHT**	**5bLT**	**5c**
Emp. formula	$C_{24}H_{15}N_3O$	$C_{29}H_{17}N_3O{\cdot}0.5(CHCl_3)$	$C_{29}H_{17}N_3O{\cdot}0.5(CHCl_3)$	$C_{23}H_{12}N_4O_3$
Fw	361.39	483.14	483.14	392.37
T [K]	100	293	160	100
space group	*Pbca*	*P*-1	*P*-1	*I*2/*a*
a [Å]	11.3181(2)	8.0034(6)	12.1617(5)	24.8719(5)
b [Å]	12.4550(2)	12.3093(12)	13.3458(5)	5.80280(9)
c [Å]	24.9296(4)	12.4079(10)	15.9128(7)	27.2343(6)
α [°]	90	77.473(8)	114.311(4)	90
β [°]	90	78.838(7)	92.757(3)	116.219(3)
γ [°]	90	87.836(7)	98.816(4)	90
V [Å^3]	3514.25(10)	1170.70(18)	2308.13(18)	3526.21(13)
Z	8	2	4	8
ρ_{calcd} [g cm^{-3}]	1.366	1.371	1.390	1.478
μ [mm^{-1}]	0.681	0.249	0.253	0.835
Crystal size [mm]	0.23 × 0.12 × 0.03	0.35 × 0.30 × 0.30	0.25 × 0.20 × 0.15	0.35 × 0.03 × 0.02
2Θ range	7.09 to 133.10	3.42 to 50.05	3.38 to 50.05	7.24 to 133.16
Refls. collected	13,627	10,142	21,753	11,594
Indep. refls., R_{int}	3096, 0.0281	4136, 0.0247	8145, 0.0373	3113, 0.0290
Data/rests./params.	3096/0/255	4136/0/335	8145/0/631	3113/0/272
GOF	1.048	1.032	1.026	1.065
R_1, wR_2(all data)	0.0350, 0.0967	0.0628, 0.1740	0.0631, 0.1629	0.040, 0.0956
CCDC no.	2352573	2354481	2354482	2352575

2.4. Computational Details

Computations regarding molecular and drug-like properties on the equilibrium geometries of the synthetized compounds were performed using Spartan v. 24 software from Wavefunction, Inc., Irvine, CA, USA [58], for the conformers showing the lowest energy of each structure, in vacuum conditions, at ground state using B3LYP [59] global hybrid density functional model with basis set 6-311 G (d, p) [60]. Evaluation of druglikeness was conducted in accordance with Lipinski's rule of five [52] and Veber's guidelines [53] regarding specific properties for drug candidates.

3. Results

3.1. Synthesis

The 9-cyano-pyrrolo[1,2-*a*][1,10]phenanthrolines **5a–c** were synthesized by an efficient one-pot reaction between 1-(4-phenylphenacyl)-1,10-phenanthrolinium bromides **2a–c**, acrylonitrile and triethylamine, in the presence of TPCD, as an oxidizing agent [61]. (Scheme 1) The synthesis of bromide precursors was previously reported in the literature [26] in the N-alkylation of 1,10-phenanthroline hydrate with 2′-bromo-4′-phenylacetophenones in acetone under reflux. Compounds **5a–c** and the corresponding atom numbering are presented in Scheme 1.

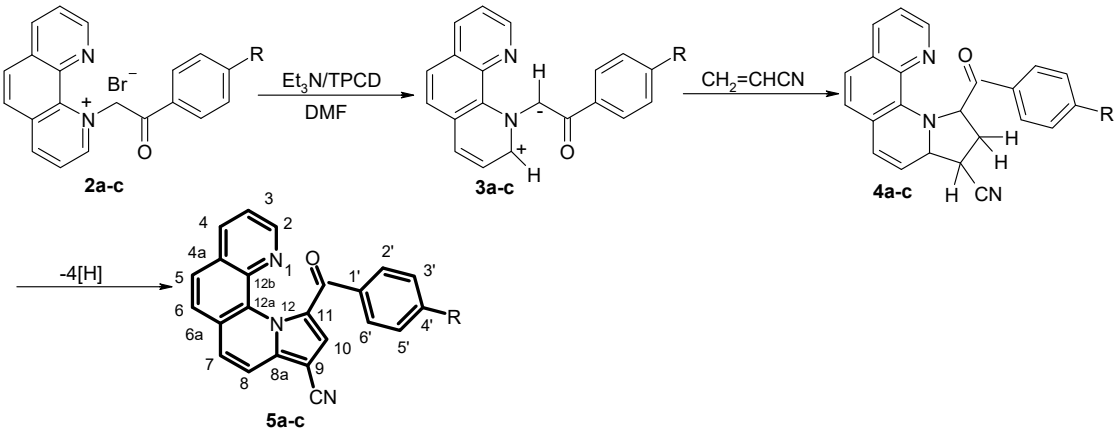

Scheme 1. The reaction pathway of 9-cyano-pyrrolo[1,2-a][1,10]phenanthrolines **5a–c**.

The synthesis of novel 9-cyano-pyrrolo[1,2-a][1,10]phenanthrolines **5a–c** consists of the aromatization of tetrahydro-pyrrolo[1,2-a][1,10]phenanthrolines **4a–c**, relatively stable in the reaction conditions, obtained by 1,3-dipolar cycloaddition of 1,10-phenanthrolinium-*N*-ylides **3a–c** with acrylonitrile, using TPCD as oxidizing agent [61].

The structures of the new compounds were elucidated by NMR spectroscopy, which confirmed the substituted 9-cyano pyrrolophenanthroline framework. The H-10 hydrogen atom appears as a singlet in the range 7.36–7.41 ppm. The most deshielded protons are H-2 and H-4 in the free pyridine ring of the phenanthroline system. The benzoyl moiety presents the signals of a *para* substitution pattern. The C atom in the CN group appears in the range 115–116 ppm. The C=O group appears in the region 183.8–184.4 ppm as the most deshielded C-atom.

3.2. X-ray Crystallography

The results of X-ray structural analyses for **5a**, **5bHT, 5bLT** and **5c** are illustrated in Figure 1, while the geometric parameters are summarized in Table S1. Compound **5b** crystallized from chloroform solution as a semisolvate. This triclinic semisolvate on cooling undergoes a phase transition to another triclinic phase with a unit cell twice as large. Upon transition, ordering of the solvent molecules takes place.

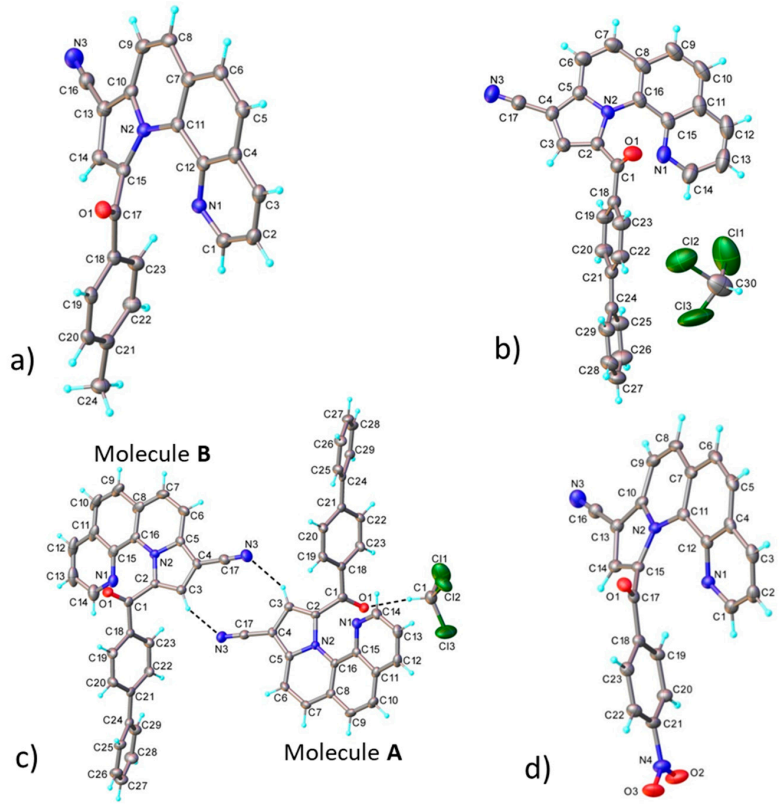

Figure 1. The asymmetric parts in the crystal structures of **5a** (**a**), **5bHT** (**b**), **5bLT** (**c**) and **5c** (**d**) showing atom labeling and thermal ellipsoids at the 50% probability level. H-bond parameters for **5bLT**: C3A-H···N3B [C3A-H 0.95 Å, H···N3B 2.64 Å, C3A···N3B 3.450(4) Å, ∠C3AHN3B 144.0°; C3B-H···N3A [C3B-H 0.95 Å, H···N3A 2.44 Å, C3B···N3A 3.280(4) Å, ∠C3BHN3A 147.7°; C1-H···O1 [C1-H 1.00 Å, H···O1 2.30 Å, C1···O1 3.232(4) Å, ∠C1HO1 155.5°.

As was to be expected, by analogy with the structures of other 1-acyl-pyrrolo[1,2-a][1,10]phenanthrolines [21,28,29], all studied molecules show severe overcrowding that results in their helical structure. The fused-ring system is twisted to avoid strong steric repulsions between the atoms of the terminal pyridine ring and the benzoyl substituent at the pyrrole fragment. The degree of helicity of the fused-ring system can be estimated by a dihedral angle between the planes of the terminal rings. These dihedral angles are similar and range from 19.54° in **5bHT** to 25.06° in **5c**. Despite the twisting of the fused-ring system, some intramolecular contacts remain quite short, as, for example, the non-bonding distance between the pyridine N1 and the carbonyl carbon C17 (2.513(2)-2.532(2) Å) that is ca. 0.7 Å shorter than the sum of the van der Waals radii. A steric strain associated with this short distance leads to a significant displacement (0.485–0.560 Å) of the carbonyl C17 atom from the plane of the virtually planar pyrrole ring and to a pyramidal arrangement of three bonds formed by C15. The C15 atom is displaced from the plane through N2, C14 and C17 by 0.468 Å in **5a** to 0.560 Å in **5bHT**. Due to a helical structure, the studied molecules are chiral and their two enantiomers can be assigned as P and M. Figure 1 shows P enantiomers, except **5bHT**, where both enantiomers related by the pseudo-inversion center are shown. It should be pointed out that all three compounds crystallize in centrosymmetric space groups, and therefore their crystals have to contain both enantiomeric forms of molecules (Figure S1).

All crystal structures were analysed from the point of view of short intermolecular contacts. As there are no classical hydrogen-bond donors in the studied molecules, only C-H···O, C-H···N, C-H···C and C-H···π interactions involving aromatic rings were expected among the specific intermolecular interactions influencing the crystal packing. In all cases, the carbonyl O1 atom takes part in a C-H···O contact that is shorter or equal

2.60 Å. The shortest H···O contact of 2.30 Å is found in **5bLT** where the solvent $CHCl_3$ molecule acts as a donor in hydrogen bonding. In **5a** and **5c**, C-H···O interactions involving the carbonyl group assemble the molecules into one-dimensional supramolecular arrays (Figures 2 and 3) that, in **5c**, are further extended into double chains by C-H···O interaction to the nitro group. In both crystalline phases of **5b,** C-H···O contacts involving the carbonyl group occur within centrosymmetric dimers formed via π···π stacking interactions between the phenanthroline fragments of the fused-ring system. These dimers are further assembled into 1D-supramolecular arrays via π···π stacking involving pyrrole and phenanthroline aromatic rings with centroid-to-centroid distances of 3.646 Å and 3.903 Å (Figure S2). Stacking interactions with the centroid-to-centroid distance of 3.636 Å between the inversion-center-related phenanthroline fragments of the neighboring one-dimensional supramolecular arrays are also found in **5a**. In turn, in **5c**, π···π stacking interactions involving the benzene and pyrrole rings (centroid-to-centroid distance 3.635 Å) occur within the 1D supramolecular assembly formed via C-H···O interactions (Figure 3), and C-H···π interactions between the phenanthroline fragments extend these assemblies in a 2D array. Short C-H···N contacts to the nitrile group (H···N < 2.70 Å) are absent in **5a** but are found in the remaining structures. In **5a** and **5bHT**, this interaction is generated between inversion-center-related molecules, resulting in dimers, whereas, in **5bLT**, the molecules in dimer are related by the pseudoinversion center and the two H···N distances of 2.44 and 2.64 Å differ significantly (Figure 1c).

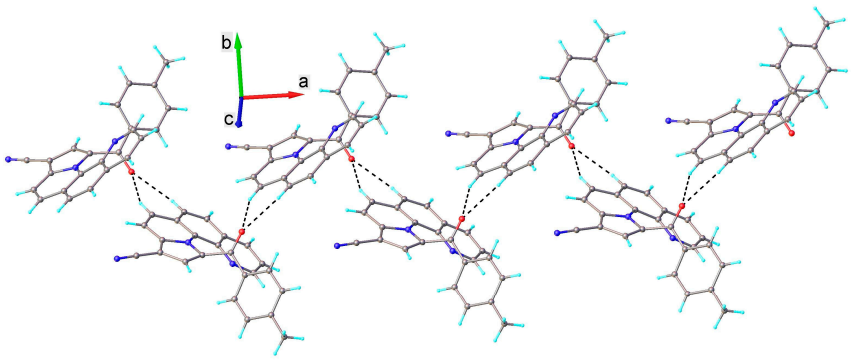

Figure 2. View of 1D supramolecular chain in the crystal structure of **5a**. H-bond parameters: C6-H···O1 [C6-H 0.95 Å, H···O1 2.60 Å, C6···O1(x − 1, 1.5 − y, 1 − z) 3.410(2) Å, ∠C6HO1 143.9°; C8-H···O1 [C8-H 0.95 Å, H···O1 2.36 Å, C8···O1(x − 1, 1.5 − y, 1 − z) 3.232(2) Å, ∠C8HO1 152.8°.

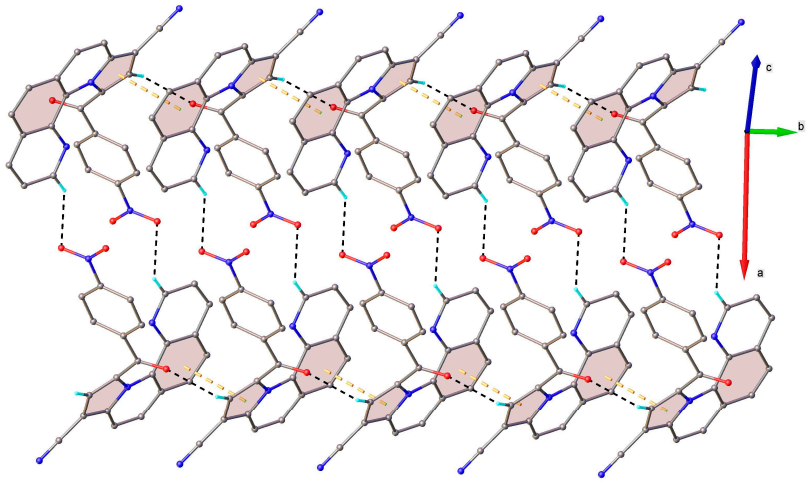

Figure 3. View of 1D supramolecular chain in the crystal structure of **5c**. H-bonds parameters: C1-H···O2 [C6-H 0.95 Å, H···O2 2.51 Å, C1···O2(1 − x, 1 − y, 1 − z) 3.300(2) Å, ∠C1HO2 140.9°; C14-H···O1 [C14-H 0.95 Å, H···O1 2.41 Å, C14···O1(x, 1 + y, z) 3.101(2) Å, ∠C14HO1 129.6°. Centroid-to-centroid contacts are shown in dashed orange lines.

3.3. Hirshfeld Surface Analysis

Hirshfeld surfaces (HF) [62] generated for compounds **5a–c** using CrystalExplorer [63] visually display the main interactions in the supramolecular structures. The red spots in d_{norm} mode present the locations of the non-covalent contacts with distances under the van der Waals radii. The most relevant interactions represented by red spots (contact distances below the sum of the vdW radii) and are mainly visible (Figure 4) for the hydrogen bonds discussed in the X-ray chapter but also for short C···C or H···C contacts (π-stacking or C-H···π). For compounds **5a** and **5bLT**, the Shape index surfaces present the complementary spots specific for π···π interactions involving the inner rings (II and III) of the pyrrolophenanthroline skeleton. This is enhanced by the curvedness surfaces, which confirm that the two rings are the most planar (Figure 4). Compound **5c**, however, does not present π···π contacts in the Shape index surface (Not shown here), even if the Hirshfeld present two red spots for short C···C contacts. These contacts might be enforced by the other strong non-covalent contacts, the distances between the ring III and ring I being 3.635 Å and the dihedral angle between the ring planes being 14.46○. However, for such a small angle and distances, one might consider a π···π interaction to occur.

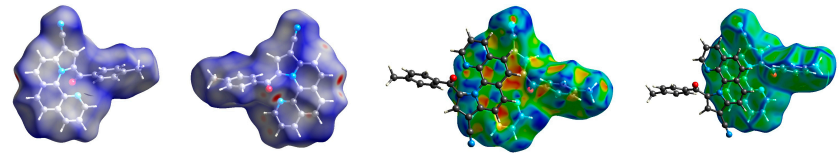

5a

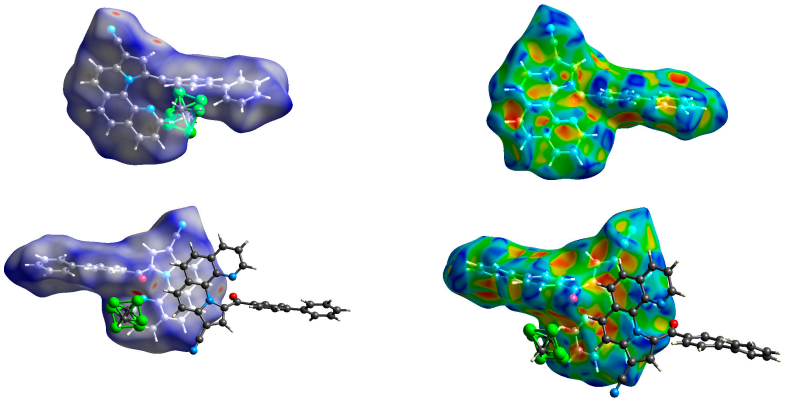

5bHT-just for illustration

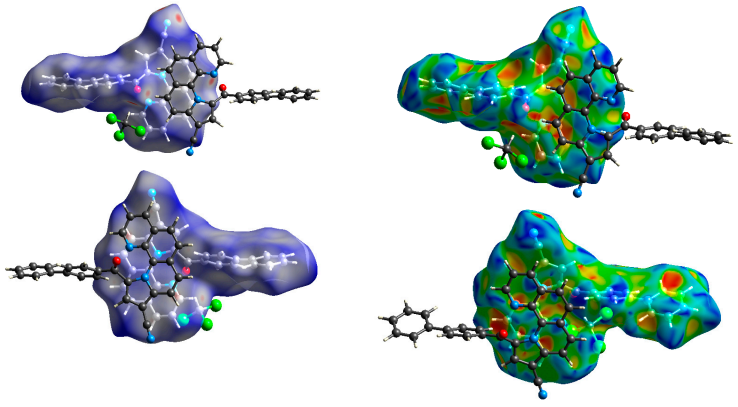

5bLT-P

Figure 4. *Cont.*

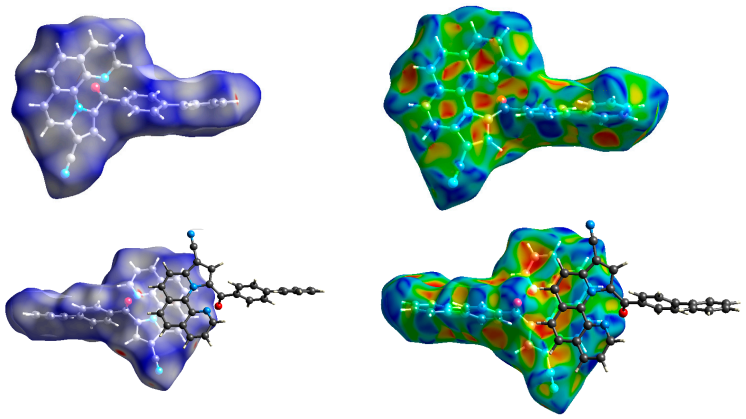

5bLT-M

Red spots: H-bonds and C···C short contacts

Complementarity zones (red/blue) and curvedness confirm π-stacking implied by the short C···C contacts

Red spots: CH···π and H-bonds

H-bond and short C···C contacts (possible π-π)

5c

Figure 4. Hirshfeld surfaces of compounds **5a–c** generated as d_{Norm}, ShapeIndex and curvedness (**5a**).

The most numerous contacts, as extracted from the Hiershfild surface, are statistically H···H contacts, which are similar (Figure 5) for **5a** and **5bLT** and present the same ratios for all the evaluated contacts. However, **5c**, due to the introduction of the NO_2 group, presents a steep decrease in H···H contacts and an increase in O···H contacts from around 7–8% for **5a,b** to 25.5% for **5c**. The statistical landscape of interactions in the Hirsfeld surface is a qualitative description and not a quantitative one. For example, N···H contacts are the strongest in compound **5b**, which presents the lowest percentage of interactions (10.6% compared to 13.3%-**5a** and 12.7%-**5c**). However, the HF surfaces and fingerprint plots are important descriptors of possible binding modes of such molecules in view of their further evaluation as potential bioactive molecules. There is no difference between the two helical enantiomers P and M in the HF percentages, with the exception of **5bLT**, where one enantiomer shares more Cl···H contacts with the chloroform solvent.

An interesting aspect in the crystal landscape of such compounds is the presence of helical chirality devising the presence of the P and M helicoidal enantiomers (Figure 6). As in the case of many helicene-like molecules, this helical chirality is induced by the presence of four or more than four ortho-condensed rings [22,64]. In structures with less condensed rings, such as pyrrolophenanthrolines, the helicoidal shape of the molecules can be induced by the presence of bulky substituents in the "Bay-region" of the molecule [21].

However, in the case of pyrrolophenanthrolines, intriguing intramolecular short-contacts were observed [27,29] between the nitrogen in ring IV and the carbon atom in the C=O from the benzoyl moiety, raising the intuition that the pitch of the helix can be influenced by an interplay of this apparently attractive force and the repulsion forces generated by the molecular strain. In this case, this non-covalent interaction might be of type lp-π between the free electrons of the N atom and the empty π-orbital of the C=O group. Such kinds of bonds are typical, for example, in protein folding due to C=O···C=O

interactions [65] (where one lp is donated by O instead of N). We measured the effect of this interaction using the value of the dihedral angle between the rings I and IV versus the contact distance between the N and C atom from C=O (Table 2). The results were not very conclusive, but it appears that such kinds of interactions can be further investigated as the measured contact lengths compared to sum of vdW radii could imply strong interactions. Another conceptual proof of this interaction might be given by the deformation of the carbonyl bond with the C atom going outside the C=O bond (pyramidalization). Also, a strong H-bond in the structure of CSD: ZIPQUM [38] leads to an increase in the molecular deformation. However, the negative correlation of the data in Table 2 shows that other effects are to be considered also.

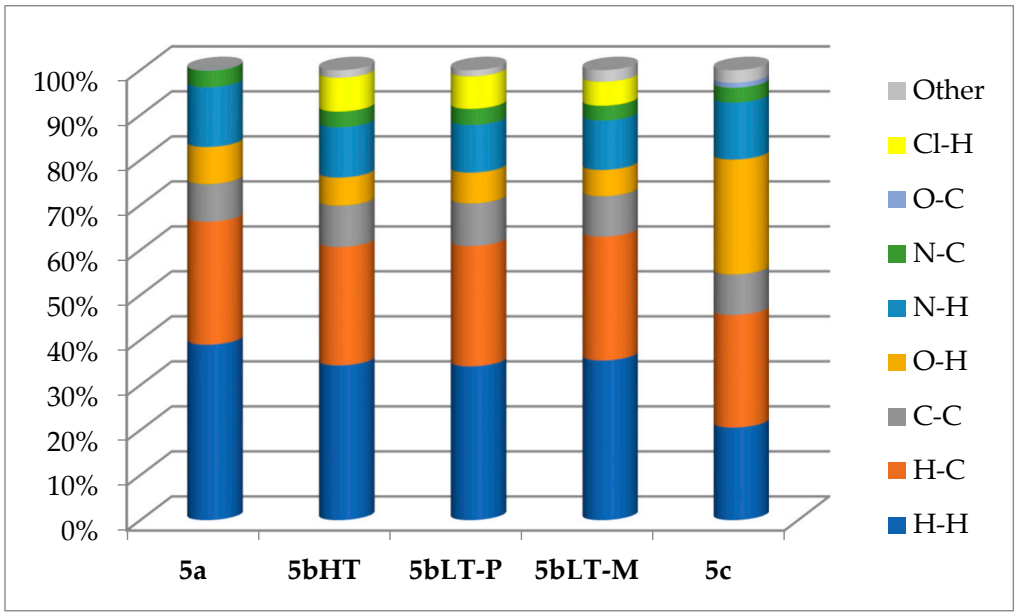

Figure 5. Percentage interactions for compounds **5a**–**c** extracted from their contribution to the HF surface. **5bHT** is exemplified for information; **5bLT** presents both enantiomers, as, beside the helix directions, the two enantiomers present some other particularities due to the interaction with $CHCl_3$ solvent.

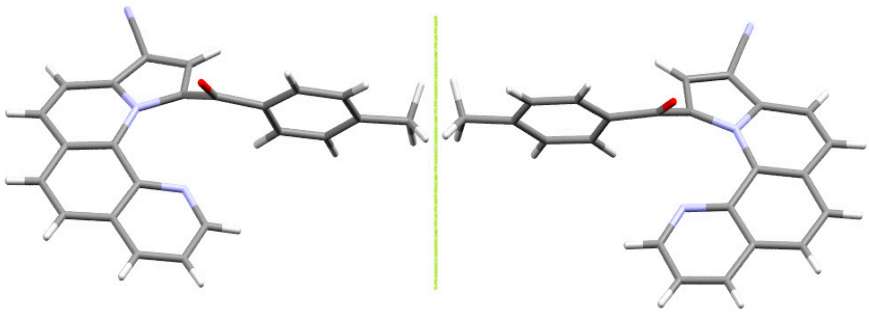

Figure 6. Mirror image of the two helical enantiomers of compound **5a**.

The helicoidal distortion of the molecules can influence the pitch of the helix and thus the structural similarity with bioactive molecules, such was the recent case of cholchicine mimick [5]-helistatin, the first known helicene showing real bioactive potential in relation with actual commercial drugs [66].

Table 2. Dihedral angles vs. distance between the N atom from pyridine ring and the C=O in the benzoyl moiety.

Compound	Dihedral Angle ○	d (C, N), Å	% Sum of vdW Radii
5a	21.11	2.529	77.82
5bLT-A	20.54	2.532	77.91
5bLT-B	19.80	2.514	77.35
5c	25.06	2.527	77.75
4-CNBenzoyl [19]	21.74	2.532	77.91
Benzoyl [19]	20.53	2.553	78.55
4-MeOBenzoyl [19]	20.82	2.551	78.49
4-HexylBenzoyl [19]	26.62	2.585	79.54
AQIKER [20b]	24.16	2.436	74.95
QAQCIV [21c]	18.81	2.513	77.32
ZIPQUM [24a]	25.54	1.8513	67.32

3.4. Druglikeness Assessment

In Figure 7, the representation of the electrostatic potential maps is given, varying from blue (the most positive values) to red (the most negative values). The potential increases in the order: red < orange < yellow < green < blue. For structure **5a**, values of the electrostatic potential range from 141.24 kJ·mol^{-1} to −209.66 kJ·mol^{-1}, for **5b**, between 130.72 kJ·mol^{-1} and −208.91 kJ·mol^{-1}, and for **5c**, the values vary from 157.19 kJ·mol^{-1} to −194.19 kJ·mol^{-1}. The less negative regions are overlapping the oxygen atoms.

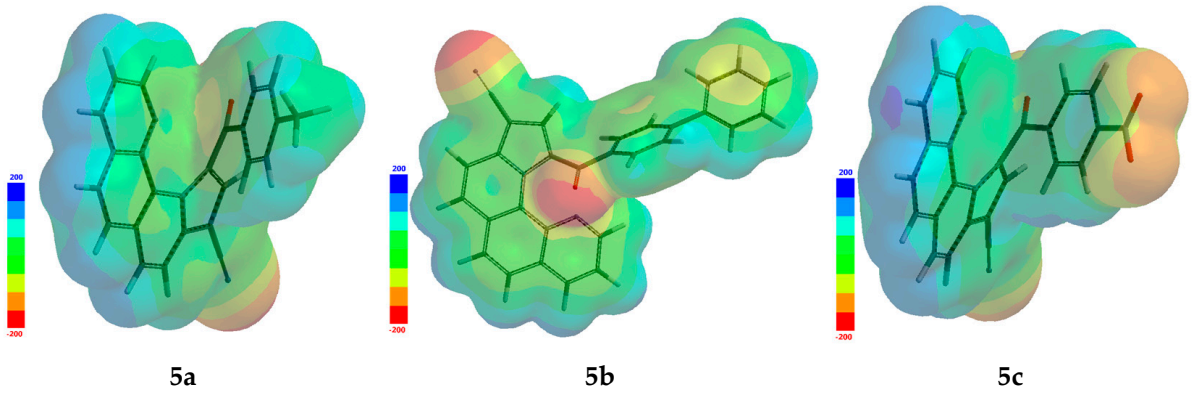

Figure 7. Electrostatic potential maps for compounds **5a**–**c**.

3.5. Quantum Reactivity Parameters Calculated from FMO Predicted Energy Levels

Regarding the molecular properties assessment, in order to evaluate the potential suitability of compounds for further development, from the point of view of druggability and oral bioavailability, by applying property filters stated by Lipinski's rule of five (RO5), it can be observed that all structures, except **5c**, exhibit one violation to RO5 in terms of hydrophilicity/lipophilicity balance, as shown from the values of *logP* listed in Table 3. Values of *logP* greater than five suggest highly lipophilic compounds. This fact severely impacts on bioavailability and will require further special pharmaceutical formulations to increase the penetration in the physiological environment and to reduce the non-polar character of these compounds. Among the three structures, **5c** is the most hydrophilic structure and **5b** is the most hydrophobic structure, as expected, due to the phenyl substituent (R). Although other requirements of RO5 are met (mass, number of hydrogen bond donor's and acceptors) for **5a** and **5b** structures, and adding the conformity with the Veber rule concerning the total polar surface area and the number of rotatable bonds, keeping in mind the fact that it represents only one minor step in drug assessment, all compounds can be further considered as leads for development and investigation of their pharmaceutical potential. Concerning the **5c** compound, the replacement of the

R substituent on the skeleton structure with NO_2 will strongly increase the hydrophilic character and also will give the opportunity for more interactions within the active site of proteins targets due to the Lewis structure for NO_2^- and due to more hydrogen bond acceptors (HBA = 7).

Table 3. Calculated druglike properties for the investigated structures.

Property (Symbol), Units	5a	5b	5c
Molecular weight (*M*) g·mol^{-1}	361.404	423.475	392.374
Area (*A*), Å^2	366.81	431.64	371.88
Volume (*V*), Å^3	370.10	435.72	373.26
Polar surface area (*PSA*), Å^2	32.552	33.008	71.158
Water-octanol partition coefficient (*logP*)	5.53	6.72	3.33
Ovality index (*OI*)	1.47	1.55	1.48
Polarizability (α), 10^{-30}·m^3	70.56	75.87	70.89
Minimum electrostatic potential, kJ·mol^{-1}	−209.66	−208.91	−194.19
Maximum electrostatic potential, kJ·mol^{-1}	141.24	130.72	157.19
Dipole moment (D), Debye	9.79	7.01	7.92
Number of hydrogen bond donors (*HBD*)	0	0	0
Number of hydrogen bond acceptors (*HBA*)	4	4	7

Additionally, predictive data for the global chemical reactivity of the investigated compounds are obtained from the frontier molecular orbitals's energy levels, as depicted in Figure 8, from their values given in Table 4. The quantum reactivity parameters are calculated according to Koopman's' theorem [67,68], which indicated relationships for the ionization potential (*I*) and the electron affinity (*A)* as the negative of HOMO and LUMO energies, respectively. Pearson's Hard and Soft Acids [69,70] is basis for calculation of the softness (σ) and hardness (η) parameters. The electronic reactivity (χ) is calculated according the Maximum Hardness Principle (MHP) [70]. The electrophilicity index (ω), is obtained from an equation stated by Parr R.G and collaborators [71]. The HOMO-LUMO energy gap is a measure of the kinetic stability and reactivity of molecules. According the calculated values, among the investigated compounds, the **5b** derivative seems to be the more stable, revealing the larger energy gap (3.62 eV), and **5c** is the most reactive, presenting the smaller energy gap (3.23 eV).

Table 4. FMO distribution and energy levels for compounds **5a–c**.

Parameter	Formula	5a	5b	5c
Energy of the HOMO orbital (E_{HOMO}), eV		−5.95	−5.92	−6.26
Energy of the LUMO orbital (E_{LUMO}), eV		−2.40	−2.30	−3.03
Ionization potential (*I*), eV	$I = -E_{HOMO}$	5.95	5.92	6.26
Electron affinity (*A*), eV	$A = -E_{LUMO}$	2.40	2.30	3.03
FMO energy gap (ΔE), eV	$\Delta E = I - A$	3.55	3.62	3.23
Electronegativity (χ), eV	$\chi = (I + A)/2$	4.175	4.11	4.645
Global hardness (η), eV	$\eta = (I - A)/2$	1.775	1.81	1.615
Softness (σ), eV^{-1}	$\sigma = 1/\eta$	0.563	0.553	0.619
Global electrophilicity index, D·eV^{-1}	$\omega = \mu^2/2\eta$	26.998	13.575	19.420

The compounds are rather stable, and their non-covalent interactions in crystalline phase validated by the ESP provide insightful information regarding the affinity of the CN group as being pharmacophore or other possible interactions mainly driven by hydrogen bonds (given by the number of hydrogen bonds acceptors). The compounds **5a–c** present large molecular masses and high *logP* values which might need further formulation studies in order to increase their bioavailability. Given the potential of such compounds confirmed by recent studies [8–14], and the potential use of the molecular distortion in mimicking com-

mercial drugs [66], the new compounds are suitable for further expanding their structural diversity and investigating their potential anti-cancer or antibiotic properties.

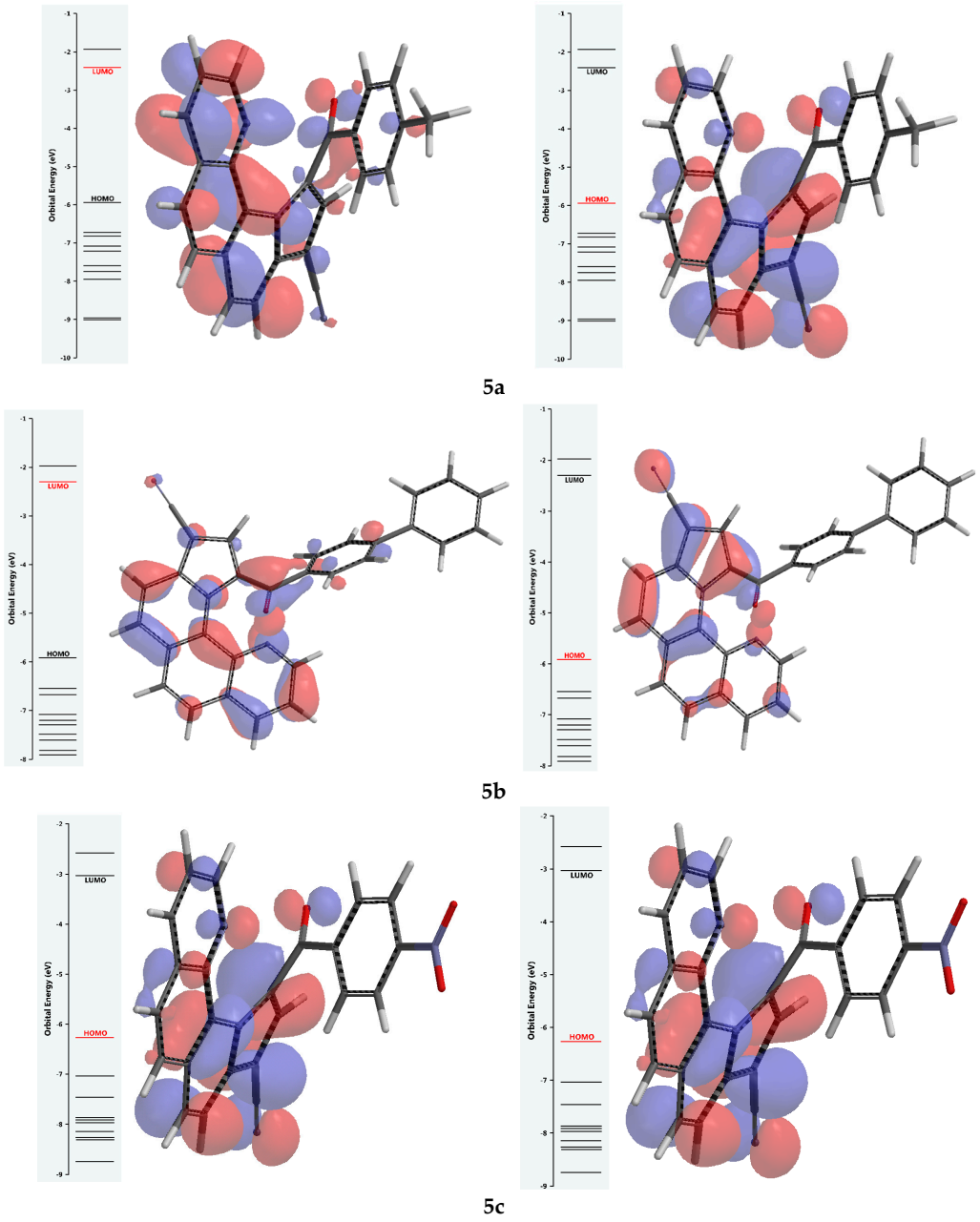

Figure 8. FMO distribution and energy levels for compounds **5a**–**c**.

4. Conclusions

In conclusion, we have synthesized and structurally characterized three new 9-cyano-pyrrolo[1,2-*a*][1,10]phenanthrolines and investigated their supramolecular interactions, extracted from X-ray single crystal diffraction analysis, with the aim of analyzing their potential supra-molecular binding sites and binding patterns. The helicoidal structures could present interesting properties which might infer them with bioactive properties.

Supplementary Materials: The following supporting information can be downloaded at: https://www.mdpi.com/article/10.3390/sym16070911/s1, Figure S1: Overlayed molecules illustrating the helical chirality for **5a** (a), **5b** (b) and **5c** (c).; Figure S2: View of 2D supramolecular layer in the crystal

structure **5b**. H bonds and centroid-to-centroid distances are shown in dashed black and orange lines, respectively; Table S1: Bond distances (Å) and angles (°).

Author Contributions: Conceptualization, F.D., M.C. and M.M.P.; methodology, F.D., M.C. and M.M.P.; software, M.M.P., S.S. and A.S.; validation, F.D., M.C., M.M.P., S.S., M.G., A.S. and M.R.; formal analysis, F.D., M.C. and C.D.; investigation, M.M.P., S.S., M.G. and A.S.; resources, F.D. and M.C.; data curation, F.D., M.C., M.M.P., S.S., A.S., M.R. and N.D.B.; writing—original draft preparation, F.D., M.C., M.M.P., S.S. and A.S.; writing—review and editing, F.D., M.C., M.M.P., S.S. and A.S.; visualization, F.D., M.C., M.M.P., S.S., A.S. and M.R.; supervision, F.D. All authors have read and agreed to the published version of the manuscript.

Funding: This research received no external funding.

Data Availability Statement: Raw data are available from the authors upon reasonable request.

Conflicts of Interest: The authors declare no conflicts of interest.

References

1. Vitaku, E.; Smith, D.T.; Njardarson, J.T. Analysis of the Structural Diversity, Substitution Patterns, and Frequency of Nitrogen Heterocycles among U.S. FDA Approved Pharmaceuticals. *J. Med. Chem.* **2014**, *57*, 10257–10274. [CrossRef]
2. Dhinamkaran, I.; Padmini, V.; Ganesan, K.; Selvarasu, K. A-One Pot Four Component and Microwave-Assisted Synthesis of Pyrrolo[1,10]phenanthrolines. *ChemistrySelect* **2017**, *2*, 6154–6158. [CrossRef]
3. Accorsi, G.; Listorti, A.; Yoosaf, K.; Armaroli, N. 1,10-Phenanthrolines: Versatile building blocks for luminescent molecules, materials and metal complexes. *Chem. Soc. Rev.* **2009**, *38*, 1690–1700. [CrossRef]
4. Vysotsky, M.O. Phenanthroline ligands with divergent pyridine units. *J. Chem. Res.* **2009**, *2009*, 133–136. [CrossRef]
5. Liu, T.-F.; Lin, H.-K.; Chen, L.-X.; Zhu, S.-R.; Wang, Z.-M.; Su, X.-C.; He, X.-W. Syntheses of the novel thiamacrocycles containing the 1,10-phenanthroline unit. *J. Chem. Res.* **2004**, *2004*, 374–375. [CrossRef]
6. Montalban, A.G.; Herrera, A.J.; Johannsen, J. Phenanthroline dipyrromethene conjugates: Potential building blocks for the construction of novel supramolecular architectures. *Tetrahedron Lett.* **2010**, *51*, 2917–2919. [CrossRef]
7. Maghsoodlou, M.T.; Habibi-Khorassani, S.M.; Hazeri, N.; Heydari, R.; Marandi, R.G.; Nassiri, M. The new γ-spiroiminolactone synthesis by reaction between alkyl or aryl isocyanides and 1,10-phenanthroline-5,6-dione in the presence of acetylenic esters. *J. Chem. Res.* **2006**, *2006*, 220–222. [CrossRef]
8. Danac, R.; Al Matarneh, C.M.; Shova, S.; Daniloaia, T.; Balan, M.; Mangalagiu, I.I. New indolizines with phenanthroline skeleton: Synthesis, structure, antimycobacterial and anticancer evaluation. *Bioorg. Med. Chem.* **2015**, *23*, 2318–2327. [CrossRef]
9. Al Matarneh, C.M.; Shova, S.; Mangalagiu, I.I.; Danac, R. Synthesis, structure, antimycobacterial and anticancer evaluation of new pyrrolo-phenanthroline derivatives. *J. Enz. Inhib. Med. Chem.* **2016**, *31*, 470–480. [CrossRef] [PubMed]
10. Dumitrascu, F.; Caira, M.R.; Draghici, C.; Caproiu, M.T.; Barbu, L.; Miu, B. New 1,10-phenanthroline derivatives with potential antitumoral activity. *Rev. Roum. Chim.* **2008**, *53*, 183–187.
11. Roy, S.; Hagan, K.D.; Maheswari, P.U.; Lutz, M.; Spek, A.L.; Reedijk, J.; van Wezel, G.P. Phenanthroline derivatives with improved selectivity as DNA-targeting anticancer or antimicrobial drugs. *ChemMedChem* **2008**, *3*, 1427–1434. [CrossRef] [PubMed]
12. Sall, C.; Yapi, A.-D.; Desbois, N.; Chevalley, S.; Chezal, J.-M.; Tan, K.; Teulade, J.-C.; Valentin, A.; Blache, Y. Design, synthesis, and biological activities of conformationally restricted analogs of primaquine with a 1,10-phenanthroline framework. *Bioorg. Med. Chem. Lett.* **2008**, *18*, 4666–4669. [CrossRef] [PubMed]
13. Nielsen, M.C.; Larsen, A.F.; Abdikadir, F.H.; Ulven, T. Phenanthroline- 2,9-bistriazoles as selective G-quadruplex ligands. *Eur. J. Med. Chem.* **2014**, *72*, 119–126. [CrossRef] [PubMed]
14. Wesselinova, D.; Neykov, M.; Kaloyanov, N.; Toshkova, R.; Dimitrov, G. Antitumour activity of novel 1,10-phenanthroline and 5-amino-1,10-phenanthroline derivatives. *Eur. J. Med. Chem.* **2009**, *44*, 2720–2723. [CrossRef] [PubMed]
15. Leontie, L.; Druta, I.; Danac, R.; Rusu, G.I. On the electronic transport properties of pyrrolo[1,2-a][1,10]phenanthroline derivatives in thin films. *Synth. Met.* **2005**, *155*, 138–145. [CrossRef]
16. Leontie, L.; Druta, I.; Danac, R.; Prelipceanu, M.; Rusu, G.I. Electrical properties of some new high resistivity organic semiconductors in thin films. *Prog. Org. Coat.* **2005**, *54*, 175–181. [CrossRef]
17. Al Matarneh, C.M.; Danac, R.; Leontie, L.; Tudorache, F.; Petrila, I.; Iacomi, F.; Carlescu, A.; Nedelcu, G.; Mangalagiu, I. Synthesis and electron transport properties of some new 4,7-phenanthroline derivatives in thin films. *Environ. Eng. Manag. J.* **2015**, *14*, 421–431.
18. Prelipceanu, M.; Prelipceanu, O.S.; Leontie, L.; Danac, R. Photoelectron spectroscopy investigations of pyrrolo[1,2-a][1,10]phenanthroline derivatives. *Phys. Lett. A* **2007**, *368*, 331–335. [CrossRef]
19. Cristea, M.; Răducă, M.; Shova, S.; Drăghici, C.; Neacşu, V.A.; Maganu, M.; Loredana Albotă (Barbu), L.; Dumitrescu, D.; Dumitrascu, F. Synthesis, Crystal Structure and Photoluminescent Properties of Novel 9-Cyano-Pyrrolo[1,2-a][1,10]Phenanthrolines. *Crystals* **2024**, *14*, 67. [CrossRef]
20. Dumitrascu, F.; Mitan, C.I.; Draghici, C.; Caproiu, M.T.; Raileanu, D. Primary cycloadducts of 1,10-phenanthrolinium and phthalazinium phenacylides with DMAD. *Tetrahedron Lett.* **2001**, *42*, 8379–8382. [CrossRef]

21. Dumitrascu, F.; Caira, M.R.; Draghici, C.; Caproiu, M.T.; Barbu, L.; Dumitrescu, D.G. Enhancing the helical distortion in pyrrolo[1,2-a][1,10]phenanthrolines. *Arkivoc* **2010**, *9*, 97–107. [CrossRef]
22. Dumitrascu, F.; Dumitrescu, D.G.; Aron, I. Azahelicenes and other similar tri and tetracyclic helical molecules. *Arkivoc* **2010**, *1*, 1–32. [CrossRef]
23. Eliel, E.L.; Wilen, S.H. *Stereochemistry of Organic Compounds*; Wiley: New York, NY, USA, 1994; pp. 1163–1166.
24. Dumitrascu, F.; Mitan, C.I.; Drăghici, C.; Căproiu, M.T. New pyrrolo[1,2-a][1,10]phenanthrolines with helical chirality. *Rev. Roum. Chim.* **2002**, *47*, 881–884.
25. Dumitrascu, F.; Mitan, C.I.; Drăghici, C.; Căproiu, M.T.; Răileanu, D. Helical chirality of new pyrrolo [1,2-a]([1,10]) phenanthrolines. *Rev. Chim.* **2002**, *53*, 787. [CrossRef]
26. Dumitrascu, F.; Caira, M.R.; Draghici, C.; Caproiu, M.T.; Badoiu, A. 1,3-Dipolar Cycloaddition Reactions of 1-(4-Phenylphenacyl)-1,10-phenanthrolinium N-Ylide with Activated Alkynes and Alkenes. *Molecules* **2005**, *10*, 321–326. [CrossRef] [PubMed]
27. Dumitrascu, F.; Draghici, C.; Caira, M.R.; Badoiu, A.; Barbu, L.; Cristea, M. 1,3-Dipolar cycloaddition reactions of 1-(3-nitrophenacyl)-1,10-phenanthrolinium N-ylide with activated alkynes. *Arkivoc* **2005**, *10*, 165–173. [CrossRef]
28. Dumitrascu, F.; Caira, M.R.; Drăghici, C.; Căproiu, M.T.; Barbu, L.; Bădoiu, A. Helical chirality of pyrrolo[1,2-a][1,10]phenanthroline derivatives. *J. Chem. Crystallogr.* **2005**, *35*, 361–365. [CrossRef]
29. Dumitrascu, F.; Caira, M.R.; Draghici, C.; Caproiu, M.T. Crystal Structure of a New Pyrrolo[1,2-a][1,10]phenanthroline Derivative. *Anal. Sci. X-ray Struct. Anal. Online* **2007**, *23*, X13–X14. [CrossRef]
30. Danac, R.; Rotaru, A.; Drochioiu, G.; Druta, I. Synthesis of Novel Phenanthroline Derivatives by 3+2 Dipolar Cycloadition Reaction. *J. Heterocycl. Chem.* **2003**, *40*, 283–287. [CrossRef]
31. Danac, R.; Constantinescu, M.; Rotaru, A.; Vlahovici, A.; Cretescu, I.; Druta, I. Study of Dipolar 3+2 Cycloaddition Reaction of 1,10-Phenanthrolinium Ylides to Activated Alkenes. *Rev. Chim.* **2005**, *56*, 85–88.
32. Dumitrascu, F.; Caira, M.R.; Draghici, C.; Caproiu, M.T.; Barbu, L. Isolation and X-Ray Structure of an Intermediate in 1,3-Dipolar Cycloaddition of 1,10-Phenanthrolinium N-Ylides with Alkynes: 1,2-Dihydropyrrolo-[1,2-a][1,10]phenanthroline. *Rev. Chim.* **2009**, *60*, 851–854.
33. Dürüst, Y.; Sağırlı, A.; Fronczek, F.R. Regioselective 1,3-dipolar cycloaddition of phenanthrolinium N-ylides to substituted arylidene oxazolones. *Mol. Divers.* **2011**, *15*, 799–808. [CrossRef] [PubMed]
34. Liu, Z.M.; Fang, J.; Yan, C.G. Diastereoselective Synthesis of 1,10-Dihydropyrrolo[1,2-a][1,10]phenanthroline Derivatives via 1,3-Dipolar Cycloaddition Reaction. *Chem. Res. Chin. Univ.* **2013**, *29*, 1089–1093. [CrossRef]
35. Paira, R.; Anwar, T.; Banerjee, M.; Bharitkar, Y.P.; Mondal, S.; Kundu, S.; Hazra, A.; Maulik, P.R.; Nirup, B.; Mondal, N.B. Copper–phenanthroline catalysts for regioselective synthesis of pyrrolo[3′,4′:3,4]pyrrolo[1,2-a]furo-quinolines/phenanthrolines and of pyrrolo[1,2-a]phenanthrolines under mild conditions. *Beilstein J. Org. Chem.* **2014**, *10*, 692–700.
36. Al Matarneh, C.M.; Ciobanu, C.I.; Apostu, M.O.; Mangalagiu, I.I.; Danac, R. Cycloaddition versus amidation in reactions of 2-amino-2-oxoethyl-phenanthrolinium ylides to activated alkynes and alkenes. *C. R. Chim.* **2018**, *21*, 1–8. [CrossRef]
37. Al-Matarneh, C.M.; Rosca, I.; Shova, S.; Danac, R. Synthesis and properties of new fused pyrrolo-1,10-phenanthroline type derivatives. *J. Serb. Chem. Soc.* **2021**, *86*, 901–915. [CrossRef]
38. Marandi, G.; Hazeri, N.; Maghsoodlou, M.T.; Habibi-Khorassani, S.M.; Torbati, N.A.; Rostami-Charati, F.; Skelton, B.W.; Makhad, M. Synthesis of Cyano-pyrrolo[1,2-a][1,10]phenanthroline Derivatives Using a Multicomponent Condensation. *J. Heterocycl. Chem.* **2013**, *50*, 568–572. [CrossRef]
39. Kitahara, Y.; Mizuno, T.; Kubo, A. Synthetic studies of benzo[b]pyrrolo[4,3,2-de][1,10]phenanthroline. *Tetrahedron* **2004**, *60*, 4283–4288. [CrossRef]
40. Li, M.; Lv, X.-L.; Wen, L.-R.; Hu, Z.-Q. Direct solvent-free regioselective construction of pyrrolo[1,2-a][1,10]phenanthrolines based on isocyanide-based multicomponent reactions. *Org. Lett.* **2013**, *15*, 1262–1265. [CrossRef]
41. Heydari, R.; Tahamipour, B. Highly regioselective synthesis of dicyano-8a,10,11-tetrahydropyrrolo [1,2-a][1,10]phenanthrolines via a domino-Knoevenagel-cyclization. *Chin. Chem. Lett.* **2011**, *22*, 1281–1284. [CrossRef]
42. Tahamipour, B.; Heydari, R.; Torbati, N.A.; Ziyaadini, M.; Graif, C. Diastereoselective synthesis and X-ray structure of new stable dicyano(8aRS,10SR,11SR)-9,9-dicyano-10-aryl-11-benzoyl-8a,9,10,11-tetrahydropyrrolo[1,2-a][1,10]phenanthrolines. *J. Chem. Res.* **2011**, *35*, 329–332. [CrossRef]
43. Heydari, R.; Tahamipour, B.; Torbati, N.A.; Graiff, C.; Ziyaadini, M. One-pot synthesis and X-ray structure of new, stable tetrahydropyrrolo [1,2-a][1,10]phenanthrolines with four diastereoisomeric centers. *Synth. Commun.* **2013**, *43*, 2031–2041. [CrossRef]
44. Al-Matarneh, C.M.; Ciobanu, C.-I.; Mangalagiu, V.; Zbancioc, G.; Danac, R. Microwave assisted synthesis of six-member ring azaheterocycles and their antimycobacterial and anticancer evaluation. *Rev. Chim.* **2020**, *71*, 287–293. [CrossRef]
45. Al Matarneh, C.M.; Amarandi, R.M.; Craciun, A.M.; Mangalagiu, I.I.; Zbancioc, G.; Danac, R. Design, Synthesis, Molecular Modelling and Anticancer Activities of New Fused Phenanthrolines. *Molecules* **2020**, *25*, 527. [CrossRef]
46. Fleming, F.F.; Yao, L.; Ravikumar, P.C.; Funk, L.; Shook, B.C. Nitrile-containing pharmaceuticals: Efficacious roles of the nitrile pharmacophore. *J. Med. Chem.* **2010**, *53*, 7902–7917. [CrossRef] [PubMed]
47. Wang, X.; Wang, Y.; Li, X.; Yu, Z.; Song, C.; Du, Y. Nitrile-containing pharmaceuticals: Target, mechanism of action, and their SAR studies. *RSC Med. Chem.* **2021**, *12*, 1650–1671. [CrossRef] [PubMed]
48. Wang, J.; Hong, L. Application of nitrile in drug design. *Chin. J. Org. Chem.* **2012**, *32*, 1643–1652. [CrossRef]

49. Vasile (Corbei), A.-A.; Ungureanu, E.-M.; Stanciu, G.; Cristea, M.; Stefaniu, A. Evaluation of (Z)-5-(Azulen-1-ylmethylene)-2-thioxothiazolidin-4-ones Properties Using Quantum Mechanical Calculations. *Symmetry* **2021**, *13*, 1462. [CrossRef]
50. Stefaniu, A.; Pirvu, L.C. In Silico Study Approach on a Series of 50 Polyphenolic Compounds in Plants; A Comparison on the Bioavailability and Bioactivity Data. *Molecules* **2022**, *27*, 1413. [CrossRef]
51. Pirvu, L.C.; Neagu, G.; Albulescu, A.; Stefaniu, A.; Pintilie, L. Potential Benefits of Dietary Plant Compounds on Normal and Tumor Brain Cells in Humans: In Silico and In Vitro Approaches. *Int. J. Mol. Sci.* **2023**, *24*, 7404. [CrossRef]
52. Lipinski, C.A.; Lombardo, F.; Dominy, B.W.; Feeney, P.J. Experimental and computational approaches to estimate solubility and permeability in drug discovery and development settings. *Adv. Drug Deliv. Rev.* **2001**, *46*, 3–26. [CrossRef]
53. Veber, D.F.; Johnson, S.R.; Cheng, H.Y.; Smith, B.R.; Ward, K.W.; Kopple, K.D. Molecular properties that influence the oral bioavailability of drug candidates. *J. Med. Chem.* **2002**, *45*, 2615–2623. [CrossRef] [PubMed]
54. Rigaku Oxford Diffraction. *CrysAlis Pro Software System*; Rigaku Corporation: Oxford, UK, 2015; CrysAlis Pro v. 1.171.38.46.
55. Sheldrick, G.M. SHELXT—Integrated Space-Group and Crystal-Structure Determination. *Acta Crystallogr. Sect. A Found. Crystallogr.* **2015**, *71*, 3–8. [CrossRef] [PubMed]
56. Sheldrick, G.M. Crystal Structure Refinement with SHELXL. *Acta Crystallogr. Sect. C* **2015**, *71*, 3–8. [CrossRef] [PubMed]
57. Dolomanov, O.V.; Bourhis, L.J.; Gildea, R.J.; Howard, J.A.K.; Puschmann, H. OLEX2: A Complete Structure Solution, Refinement and Analysis Program. *J. Appl. Crystallogr.* **2009**, *42*, 339–341. [CrossRef]
58. Shao, Y.; Molnar, L.F.; Jung, Y.; Kussmann, J.; Ochsenfeld, C.; Brown, S.T.; Gilbert, A.T.B.; Slipchenko, L.V.; Levchenko, S.V.; O'Neill, D.P.; et al. Advances in methods and algorithms in a modern quantum chemistry program package. *Phys. Chem. Chem. Phys.* **2006**, *8*, 3172–3191. [CrossRef] [PubMed]
59. Lee, C.; Yang, W.; Parr, R.G. Development of the Colle-Salvetti correlation-energy formula into a functional of the electron density. *Phys. Rev. B* **1988**, *37*, 785–789. [CrossRef] [PubMed]
60. Hehre, W.J. *A Guide to Molecular Mechanics and Quantum Chemical Calculations*; Wavefunction, Inc.: Irvine, CA, USA, 2003.
61. Hu, Y.; Hu, H. A Versatile Oxidizing Agent: Tetrakis-pyridino-cobalt(II) Dichromate $Py_4Co(HCrO_4)_2$ (TPCD). Oxidations of Alcohols, Halides and Amines to Their Corresponding Carbonyl Compounds. *Synth. Commun.* **1992**, *22*, 1491–1496. [CrossRef]
62. Spackman, M.A.; Jayatilaka, D. Hirshfeld surface analysis. *CrystEngComm* **2009**, *11*, 19–32. [CrossRef]
63. Spackman, P.R.; Turner, M.J.; McKinnon, J.J.; Wolff, S.K.; Grimwood, D.J.; Jayatilaka, D.; Spackman, M.A. CrystalExplorer: A program for Hirshfeld surface analysis, visualization and quantitative analysis of molecular crystals. *J. Appl. Crystallogr.* **2021**, *54*, 1006–1011. [CrossRef]
64. Shen, Y.; Chen, C.F. Helicenes: Synthesis and applications. *Chem. Rev.* **2012**, *112*, 1463–1535. [CrossRef] [PubMed]
65. D'Arminio, N.; Ruggiero, V.; Pierri, G.; Marabotti, A.; Tedesco, C. Emerging role of carbonyl–carbonyl interactions in the classification of beta turns. *Protein Sci.* **2024**, *33*, e4868. [CrossRef] [PubMed]
66. Rushworth, J.L.; Thawani, A.R.; Fajardo-Ruiz, E.; Meiring, J.C.; Heise, C.; White, A.J.P.; Akhmanova, A.; Brandt, J.R.; Thorn-Seshold, O.; Fuchter, M.J. [5]-Helistatins: Tubulin-Binding Helicenes with Antimitotic Activity. *JACS Au* **2022**, *2*, 2561–2570. [CrossRef] [PubMed]
67. Pearson, R.G. Absolute electronegativity and hardness: Application to inorganic chemistry. *Inorg. Chem.* **1988**, *27*, 734–740. [CrossRef]
68. Yankova, R.; Genieva, S.; Halachev, N.; Dimitrova, G. Molecular structure, vibrational spectra, MEP, HOMO-LUMO and NBO analysis of $Hf(SeO_3)(SeO_4)(H_2O)_4$. *J. Mol. Struct.* **2016**, *1106*, 82–88. [CrossRef]
69. Pearson, R.G. Recent Advances in the Concept of Hard and Soft Acids and Bases. *J. Chem. Educ.* **1987**, *64*, 561–567. [CrossRef]
70. Pearson, R.G.; Songstad, J. Application of the Principle of Hard and Soft Acids and Bases to Organic Chemistry. *J. Am. Chem. Soc.* **1967**, *89*, 1827–1836. [CrossRef]
71. Parr, R.G.; Szentpaly, L.; Liu, S. Electrophilicity Index. *J. Am. Chem. Soc.* **1999**, *121*, 1922–1924. [CrossRef]